Using a multi-disciplinary approach to characterize groundwater systems in arid and semi-arid environments: the case of Biskra and Batna regions (NE Algeria)

Giorgio Ghiglieri*[a-b], Cristina Buttau[a-b], Claudio Arras[a-b], Antonio Funedda[a], Albert Soler[c], Manuela Barbieri[c], Raul Carrey[c], Cristina Domènech[c], Clara Torrentó[c], Neus Otero[c-d] , Alberto Carletti[a-b-e]

(a) Department of Chemical and Geological Science, University of Cagliari, Cittadella Universitaria di Monserrato – Blocco A – S.P. Monserrato-Sestu, km 0.700, Italy

(b) Desertification Research Group (NRD), University of Sassari, Viale Italia, 07100 Sassari, Italy

(c) Grup MAiMA, SGR Mineralogia Aplicada, Geoquímica i Geomicrobiologia, Departament Mineralogia, Petrologia i Geologia Aplicada, Facultat de Ciències de la Terra, Universitat de Barcelona (UB), C/ Martí i Franquès, s/n - 08028 Barcelona, Spain

(d) Serra Hunter Fellow, Generalitat de Catalunya, Spain

(e) Department of Agriculture, University of Sassari, Viale Italia 39, 07100 Sassari, Italy

ABSTRACT

This study presents a multi-disciplinary approach for the hydrogeological assessment and characterization of water resources in typical arid and semi-arid areas with high anthropogenic pressure, and where environmental conditions and political context prevent extensive field surveys. The use of a three-dimensional (3D) hydrogeological conceptual model, integrating hydrochemical and multi-isotope data, is proposed for the Batna and Biskra area (NE Algeria).

Geological data were assembled in 3D geological software, from which a 3D hydrogeological conceptual model was constructed, which included the delineation of groundwater flow directions. The isotopic characterization, including deuterium and oxygen isotopic composition of water (δ^2H and δ^{18}O), and tritium (^{3}H), provided information regarding recharge sources, flow pathways and residence times of groundwaters. Hydrochemical parameters, measured on the same samples, supported the interpretation of isotope data. All data were processed in a geographic information system (GIS) environment. The

effectiveness of this approach was tested on a complex system of aquifers with high hydrogeological heterogeneity. Results show the important role the tectonic setting of an area can play in the hydrogeology and hydrochemistry of its principal groundwater systems. The fault network in the study region connects different aquifers, resulting in the mixing of groundwaters. The region most influenced by geological structures is the southern part of the study area, close to Biskra city. In fact, besides a limited contribution of recharge from rain and surface water derived from flood events, the recharge of the Cenozoic aquifers seems to proceed from the ascension of deeper Cretaceous groundwaters through the fault network, as indicated by temperature, bulk chemistry and in particular $\delta^{2}H$, $\delta^{18}O$ and ^{3}H results. In contrast, results suggest that the recharge of the low mineralized Maastrichtian waters is primarily influenced by local precipitation and runoff in the mountainous northern part of the study area. Tritium content, low salinity, and bulk chemistry all suggest such waters to be a mix of pre-bomb (deeper flow-lines within the aquifer) and recent water, with no contribution from the deepest Continental Intercalaire groundwaters.

The proposed approach reduces ambiguity about the studied aquifer systems, greatly improves the conceptual understanding of their behaviour, and could provide insights into the vulnerability of the aquifers to different anthropogenic pollution phenomena. The methodology used appears to be a valid tool that could be applied to other geographical areas, to inform the design and implementation of efficient management strategies aimed at improving the quality and availability of water resources. Moreover, three-dimensional modelling methods are becoming increasingly applied to different aspects of groundwater management, to obtain a detailed picture of subsurface conditions.

Keywords: 3D hydrogeological modelling; hydrogeochemistry; water isotopes; groundwater management; Biskra-Batna, Algeria.

*Corresponding author. Tel.: +39 70 6757717; E-mail: ghiglieri@unica.it G. Ghiglieri.

1. INTRODUCTION

The North African arid and semi-arid lands of the Maghreb suffer scarce water conditions, with a rainfall rate of about 200 mm/year. Erratic behaviour of rainfall over brief time intervals often produces short and intense floods events that converge into ephemeral wadi (river) beds. Since these intermittent surface water flows are often not optimally managed, most of the potential water resources generated in the flood events are lost, providing scarce benefits for households living in villages in the semi-desert areas (de Jong et al., 2008; Ghiglieri & Carletti, 2010).

The present research was developed within the framework of the WADIS-MAR project (www.wadismar.eu), a Demonstration Project funded by the European Commission. The WADIS-MAR Project concerns the implementation of integrated water harvesting systems and the application of MAR (Managed Aquifer Recharge) in two watersheds in the Maghreb Region: Wadi Biskra in Algeria, and Wadi Oum Zessar in Tunisia. These areas are characterized by water scarcity, and overexploitation and pollution of groundwater resources; and are highly exposed to climate change risk and desertification processes (Ghiglieri et al., 2014).

Before the development of any artificial recharge facility, the viability and feasibility of the project should be established through a hydrogeological conceptual model of the site, based on geological information, aquifer properties, hydrogeochemistry and possibly isotopic data. During the last few years, techniques in three-dimensional (3D) hydrogeological model reconstruction/visualization have been improved (Butscher et al., 2017; Ghiglieri et al., 2016 and references therein), integrating different sets of data (e.g., geological, hydrogeological, geophysical). Traditional geological maps show two-dimensional (2D) distribution of superficial deposits based on the interpretation of landforms, field examination of exposed materials and information from shallow excavations or drilling. In contrast to traditional 2D geological maps, 3D geological maps and models can provide highly sophisticated and detailed geological information, and therefore offer great potential benefits to users (Touch et al., 2014). Geological 3D models are increasingly used to deepen knowledge of the subsoil. Engineers, geologists and developers can use this approach to visualize and analyse relationships between structural features and geotechnical property characteristics

within specific geological units (Zhu et al. 2013; Butscher et al., 2017). When applied to groundwater studies, 3D stratigraphic modelling allows complex geological and hydrogeological features of subsurface environments to be evaluated. Geological formations are differentiated by comparing their physical properties, vertical sequences, and lateral distribution patterns according to modern models of sediment deposition (Ghiglieri et al., 2016). The detailed distribution of the thickness, depth, lateral facies extent, stratigraphy and geometry of aquifers can be displayed by using 3D visualization software to produce multiple cross sections, block diagrams and slice maps. This provides the most complete and internally consistent picture of subsurface geology, which can help define reliable hydrogeological conceptual models, and assist in the interpretation of groundwater dynamics (Da Pelo et al., 2017; Ghiglieri et al., 2016). Such accurate 3D visualizations are also the first step toward numerical modelling of groundwater flow and transport.

Water isotopes (hydrogen, oxygen and tritium) are a powerful tool that can provide important information about recharge areas and mixing processes at a regional scale in hydrogeological basins where local and large-scale flow systems converge (Biddau et al., 2019; Palmer et al., 2007; Pittalis et al., 2018 and references therein; Puig et al., 2017). Analysis of water stable isotope fractionation by natural physico-chemical processes involving surface and groundwater can help to accurately define the parameters used in hydrogeological conceptual models (Colombani et al., 2019; Gamboa et al., 2019; Tullen et al., 2006).

The aim of the present research is to develop a methodological approach for constructing a hydrogeological conceptual model of complex aquifers systems with high hydrogeological heterogeneity, based on 3D geological reconstruction of the subsurface integrated with hydrogeological, hydrogeochemical and isotopic data of selected samples. The improved 3D information that can be obtained may be crucial to the design and development of efficient management strategies aimed at improving water resource quality and availability. In the context of arid and semi-arid regions of the Maghreb, and more generally in developing countries, the proposed approach may have useful applications due to difficulties in data collection. In the present study, we have applied it to elaborate a plausible 3D hydrogeological conceptual model in the Batna and Biskra area (NE Algeria) for evaluating the possible pathways of recharge and regional

102 groundwater circulation also as support for the design and implementation of a MAR system in an alluvial
103 aquifer near Biskra (Ghiglieri et al. 2014).
104
105 **2. DESCRIPTION OF THE STUDY AREA**
106 The study area is located in the Wilaya (province) of Biskra and Batna, in North-Eastern Algeria.
107 Geographically, the area mainly extends over the south-western slope of the Aures Mountains, at the
108 boundary of the Sahara Platform (Fig. 1).
109 The Aures Mountains represent the eastern range of the Saharan Atlas chain. Alternating mountain ridges
110 and fluvial valleys dipping towards the SW characterize the south-western slope of the Aures Mountains.
111 Streams flowing from the mountain domain to the subjacent plains, such as the El Outaya and the Zibane
112 lowland, produce extensive alluvial fan deposits. The El Outaya plain, in particular, represents a small
113 endorheic basin surrounded by Atlas reliefs. The Zibane lowland is characterized by a flat south-eastern
114 dipping surface that reaches negative elevation values corresponding to the endorheic basin of Chott
115 Melrhir (-70 m amsl).
116 The Oued el Hai Biskra is the main drainage system of the study region (Fig. 1). It has its headwaters in the
117 Belezma Mountains (2100 m amsl; Fig. 1), where a precipitation rate of between 400 and 500 mm/year is
118 recorded. It flows through the Aures domain for approximately 60 km in a NE–SW direction, receiving
119 outflow from a number of tributaries, and emerges from a morphological sluice on the Djebel Mekrizane
120 to the El Outaya Plain. Since the year 2000, this portion of the watershed has drained into the *Barrage*
121 *Fontaine des Gazelles*, an earth-filled dam with a clayey core and a total capacity of ~55 Mm^3. Subsequently,
122 the Oued el Hai-Biskra flows in a N–S direction toward the Chott Melrhir basin, receiving the contribution of
123 other tributaries like Oued bou Gatou, Oued Branis, Oued Lefrah, and Oued el Besbas. According to the
124 Köppen-Geiger climate classification (Beck et al., 2018), the Biskra and Batna regions are characterized by a
125 hot arid desert and cold semi-arid cold or cold arid steppe climate. Analysis of the annual cumulative
126 precipitation measured at the Biskra rain gauge station for the period 1974–2011 shows that precipitation
127 is extremely variable, ranging from 31.9 mm in 1993 to 407.1 mm in 2009 (www.wadismar.eu). The average

for the whole period is 131.1 mm/year. Maximum temperatures are higher than 20 °C throughout the year, reaching up to 44 °C in July and August. Minimum temperatures reach 3 °C in winter and 23 °C in summer. Similar to other geographic areas characterized by an arid and semi-arid climate, land degradation processes are the main threat for land use practices. Of the different forms of degradation, soil salinization is the main challenge to sustainable agriculture in these areas. Recent studies, based on the application of new spectral indexes of remote sensing data, have shown that there was a 53% increase in highly saline soil surface area in the period between 1984 and 2014 (Afrasinei et al., 2015, 2017).

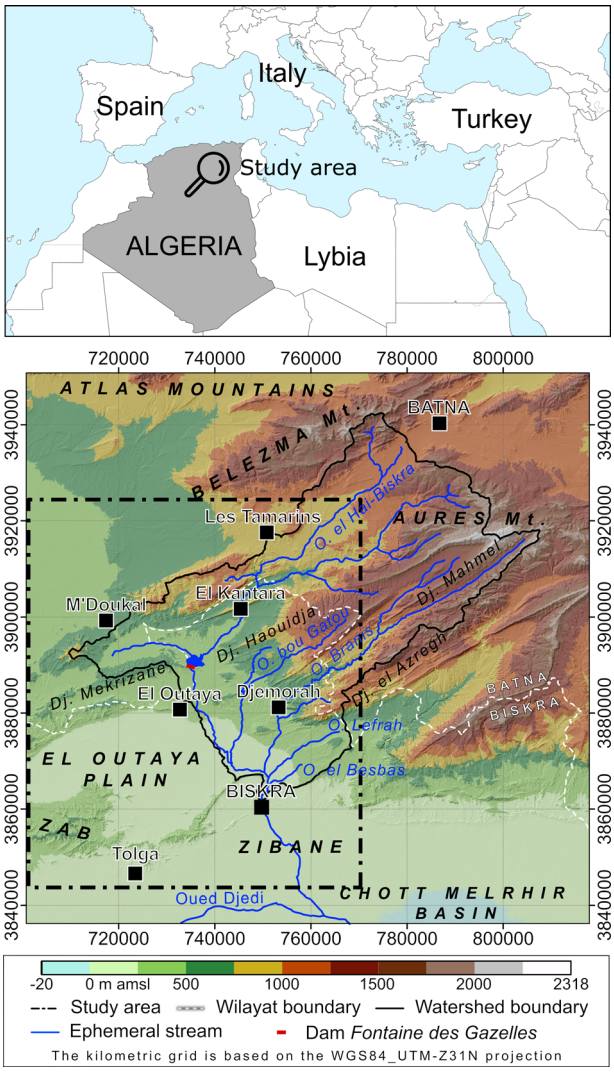

Figure 1 - Location of the study area in Northern Algeria. Geographical features of the south-western slope of the Aures Mountains (extracted from the SRTMGL1 DEM).

139 The groundwater in the Wilaya of Biskra is exploited by various sectors (domestic, agronomic, and
140 industrial use) with high and increasing demand. This situation has resulted in the depletion of the water
141 resources, with a progressive lowering of the groundwater table and an increase in salinity
142 (www.wadismar.eu).
143
144 *2.1 Geological and structural framework*
145 The study area mainly consists of Mesozoic to Cenozoic sedimentary successions (Guiraud and Bosworth,
146 1997). Alternating sequences of Triassic evaporitic gypsum and terrigenous clastic rocks represent the
147 oldest formations that outcrop in the study area (Bracène and Frizon de Lamotte, 2002). They occur due to
148 diapirism and constitute isolated reliefs, such as Djebel el Melah. The deformation history that affected
149 these successions is composed of:
150 - the "Atlas Event" (Lower Eocene-Lutetian), involving the Triassic to Lower Eocene formations. This event
151 created several folds and thrust faults orientated NE–SW, which were developed by NW–SE-trending
152 shortening, contemporary with uplift (Frizon de Lamotte et al., 2000);
153 - Relative quiescence and rapid uplift in the Miocene, characterized by sedimentation of molasse-type
154 deposits that cover the oldest formations (Bracène et al., 2002);
155 - the "Villafranchian phase" in the Miocene, characterized by N–S shortening and uplift, responsible for the
156 tilting of Miocene formations and the development of folds with an E–W axial trend (Frizon de Lamotte et
157 al., 2000).
158
159 *2.2 Hydrogeological features*
160 In the Biskra and Batna regions it is possible to recognize two hydrogeological units or aquifer systems
161 (Castany, 1982): the Complex Terminal aquifer (CTa) and the Continental Intercalaire aquifer (CIa). These
162 two units are separated by a Cenomanian impermeable level (Ci) and can be described as following. A
163 schematic diagram of the hydrogeological units is shown in Fig. 2, where the main groundwater flow
164 directions, distinguished by hydrogeological units and related recharge areas, are reported.

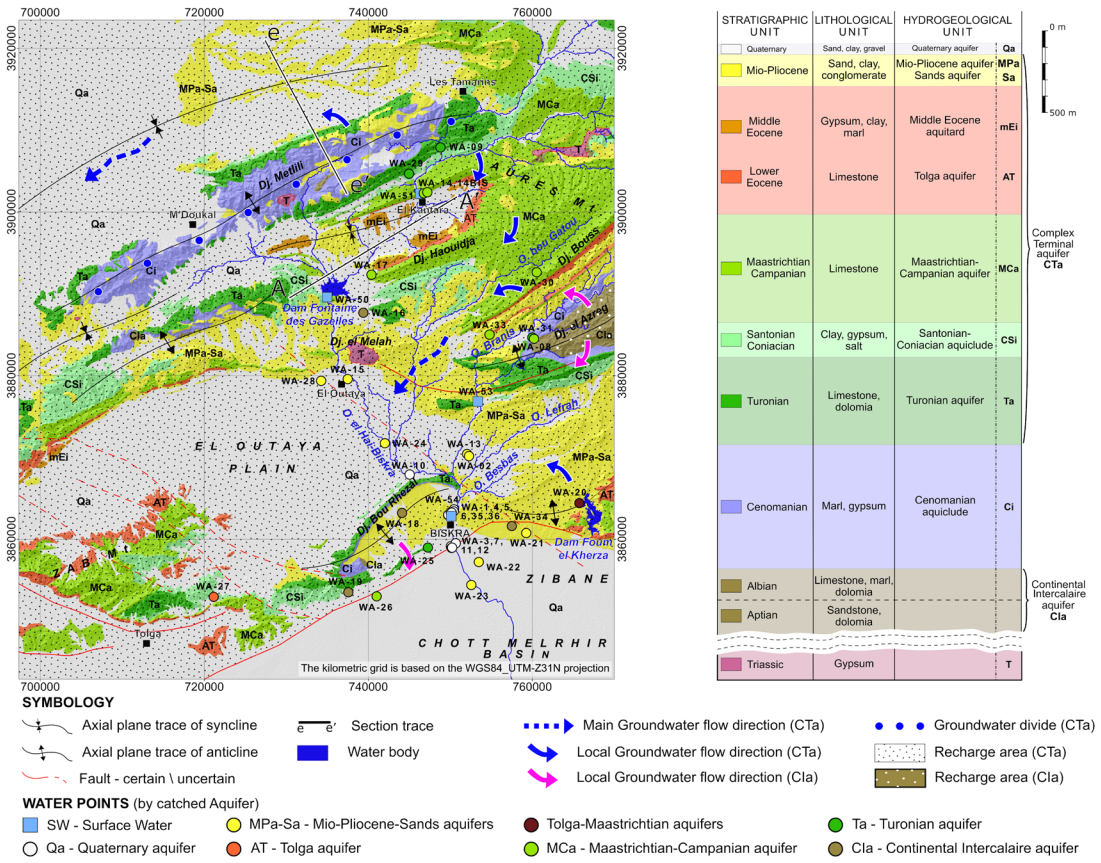

Figure 2 - Hydrogeological map of the study area. Location of the water points sampled in June 2012, May 2013 and March 2014.

Quaternary aquifer (Qa): alluvial deposits within the wadi valleys or loose sediments in the piedmont areas host the Quaternary phreatic aquifer. The thickness of the aquifer ranges from a few to tens of meters and withdrawal occurs at 1422 pumping wells, which extract a total of 60 hm^3/a (ANRH, 2008).

Complex Terminal aquifer (CTa): this aquifer represents a large hydrogeological unit composed of several minor aquifers hosted by the Upper Cretaceous to Mio-Pliocene formations (Edmunds et al., 2003). These aquifers are generally unconfined, and direct recharge could occur in the region of the Saharan Atlas, where the individual hydrogeological units crop out. Uncertainties on the intensity of erosion that took place during the Cenozoic do not allow an estimation of the thickness of the whole CTa, which includes the following aquifers:

- *Mio-Pliocene - Sands aquifer (MPa-Sa)*: in the region of Biskra and Batna this aquifer has a wide areal extension and is characterized by a succession of sand and gravel levels with local clay lenses. Heterogeneity within the deposit influences the hydraulic conductivity of the aquifer, which is highly

variable depending on location. Its thickness ranges from 100 to 300 m and the average yield is about 0.47 hm^3/a. Groundwater flow direction is toward the endorheic basin of Chott Melrhir. The MPa is the most exploited of all the aquifers listed here (ANRH, 2008);

- *Middle Eocene aquitard (mEi)*: this aquitard is represented by evaporitic and marly deposits of a lagoon environment;
- *Tolga aquifer (AT)* and *Maastrichtian-Campanian aquifer (MCa)*: limestones of the Upper Cretaceous (Campanian-Maastrichtian) to the Lower Eocene host a karst aquifer that has a total thickness ranging from 400 to 500 m;
- *Santonian-Coniacian aquiclude (CSi)*: an intercalation of evaporitic deposits, ranging in thickness from 100 to 300 meters, separates the AT and MCa from the Turonian aquifer;
- *Turonian aquifer (Ta)*: limestone and dolostone deposits host the Turonian karst aquifer that locally could be in hydraulic communication with the Limestones aquifer (AT and MCa). The Ta has a total exploitation rate of 0.5 hm^3/a;
- *Cenomanian aquiclude (Ci)*: an aquiclude level constituted by an alternation of marls and gypsum deposits of Cenomanian Age separates the CTa from the CIa.

Continental Intercalaire aquifer (CIa) extends over the whole North Africa region. It represents one of the largest confined aquifers in the world, covering a surface of about 600,000 km^2, with a potential reservoir thickness that ranges from 120 to 1000m (Castany, 1982). This aquifer is composed mainly of Lower Cretaceous deposits, with additional Triassic and Jurassic deposits in several areas. The CIa consists of several horizons with strong artesian pressure (5–25 bars) and temperatures ranging from 65 to 75 °C. In the study area, the CIa is identified both in outcrops (i.e., at the surface), and at variable depths (1600–2500 m), and is hosted by Lower Cretaceous formations (Aptian to Albian). Withdrawal rate of this aquifer is about 39 hm^3/a (ANRH, 2008).

3. MATERIALS AND METHODS

Bibliographic research and direct field surveys in any area represent the largest source of input data for scientific research and applications. In the present study, adverse environmental conditions and a particular political context made direct investigation and collection of data in situ difficult. To overcome these difficulties, with the aim of yielding a hydrogeological conceptual model, we have applied a methodological approach based on a deep analysis and reprocessing of pre-existing geological, lithological and structural data (MdH, 1980; SGA, 1962; SGA, 1972), supported by the integration of limited hydrogeological information and complemented with hydrogeological field surveys and new geochemical and isotope data from selected sampling points. The proposed multidisciplinary approach is reported in the flow chart in Fig. 3 and described in detail in Sections 3.1–3.2.

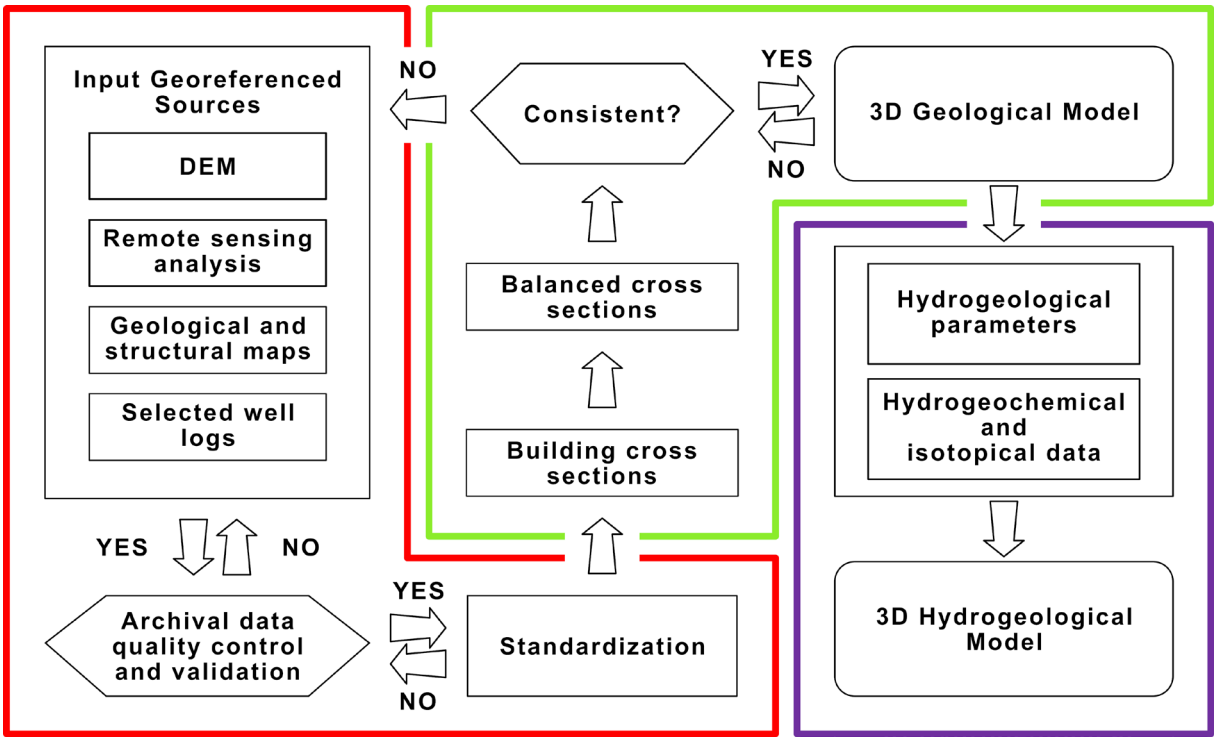

Figure 3 - Flow chart illustrating the methodological approach.

3.1. Stratigraphic analysis, data handling and 3D hydrogeological model

As a first step, surface and subsurface data were employed to reconstruct a 3D hydrogeological model. Geological and structural maps of the area were prepared on the basis of previous data and limited field surveys. These data were integrated with: aerial photographs, satellite Landsat images, the digital elevation models (DEMs) ASTER GDEM2 and SRTMGL1, existing geological maps (SGA, 1962; SGA, 1972) and 105 well

222 stratigraphic logs (MdH, 1980). The WGS84 (World Geodetic System 1984) UTM (Universal Transverse
223 Mercator) Zone 31 North was selected as the reference coordinate system. SRTMGL1 was chosen as the
224 DEM, as it has been demonstrated to be more accurate than ASTER GDEM2 in this morphological context
225 (Arras et al., 2017).
226 A RDBMS (Relational DataBaseManagement System), implemented withMicrosoft Access™software,was
227 developed to organize, store and process the collected data. A GIS (ArcGIS 10.0 - ESRI, Redmond, USA)
228 database was populated with attributes regarding geological information, topographic features, well log,
229 stratigraphy, geological age, hydrogeology, and well-casing. All the data were reclassified, integrating the
230 descriptive attributes or the lithofacies code with a standard code as an additional attribute. Validation
231 procedures and database quality control were carried out according to the criteria and strategies proposed
232 by Ross et al. (2005), which avoid the duplication of data, validate borehole location and elevation, and
233 homogenize geological information. Twenty geological sections were constructed. Twelve of these sections,
234 oriented NW–SE, and two oriented NE–SW, of length equal to 380 km, orthogonal to the main tectonic
235 structures, and evaluated for quality on the basis of the number of stratigraphic logs and other geological
236 information available along their length, were used for the reconstruction of the geological model. Another
237 6 geological sections, of length equal to 25 km, with variable orientations, were also constructed to better
238 describe and understand the geometry of structures. The geological cross sections were created manually
239 and then imported, georeferenced, and digitized within the geo-modeller.
240 An ArcGIS tool (ArcGIS eXacto Section v2.0) was used to process each geological cross-section. The software
241 package MOVE (www.mve.com/software/move, n.d) was used to verify the consistency of the 3D
242 geological model. The boreholes and the associated stratigraphy were projected onto the nearest
243 geological sections, and used to calibrate the subsurface configuration of the geological contacts. The
244 horizons representing the same contacts in the various sections were then interpolated to produce 3-D
245 geological surfaces. “Point-based Delaunay triangulation” was used as the interpolation method because of
246 its efficacy in the visualization and reconstruction of geological objects (Xue et al., 2004). The information

247 provided by hydrogeochemical and isotopic characterization at selected sampling points was also
248 integrated, producing the final 3D hydrogeological conceptual model of the study area.
249
250 *3.2. Hydrogeochemical and isotopic data*
251 *3.2.1 Field surveys*
252 Due to the size of the study area covered by the geological model, a smaller and representative area, where
253 all aquifers cited in section 2.2 were present, was selected for hydrogeochemical and isotopic
254 characterization. Within this area, 40 sampling points were considered for both chemical and isotopic
255 characterization, corresponding to 34 wells, 2 thermal springs, and 4 surface water points. Location of
256 these sampling points can be found in Fig. 2. Three field campaigns were performed, in June 2012, May
257 2013 and March 2014. Not all the points were sampled at each survey, gathering in total 57 water samples
258 (49 groundwater samples, 2 springs and 4 surface water samples). For deeper characterization of the stable
259 isotope composition of water, another 35 water samples from existing and 30 additional control points (28
260 wells, 1 spring, and 1 stream; location shown in the Supplementary data, Fig. S1) were sampled. Spring and
261 stream samples were collected directly, whereas the pumps installed at wells were used to collect
262 groundwater samples. Wells depth is shown in tables S1 and S2. Physicochemical parameters (pH,
263 temperature, and electrical conductivity - EC) were measured *in situ*, avoiding contact with the atmosphere
264 in the wells. Water samples were filtered with a Millipore® filter of 0.45 µm or 0.2 µm pore size, and
265 preserved at 4 °C in darkness prior to further analysis, following the official standard methods (APHA-
266 AWWA-WEF, 1998).
267 *3.2.2 Chemical and Isotopic Analysis*
268 Major cation and anion contents of the water samples were characterized. The anions (SO_4^{2-}, Cl^-, NO_3^-, and
269 NO_2^-) were analysed by high-performance liquid chromatography (HPLC), using a WATERS 515 HPLC pump
270 with IC-PAC Anion columns, and WESCAN and UV/VIS KONTRON detectors. For major elements (Ca, Na,
271 Mg, K), samples were filtered through a 0.2 µm Millipore® filter, acidified with 1% HNO_3^-, and analysis was
272 carried out by inductively coupled plasma-optical emission spectrometry (ICP-OES, Perkin-Elmer Optima

3200 RL). Carbonates and bicarbonates (CO_3^{2-}–HCO_3^-) were determined by a titration method using 0.05N HCl and calculated with pH 5.5 as end-point monitoring. The chemical analyses were performed in the Centres Científics i Tecnològics of the Universitat de Barcelona (CCiT-UB). The error in the measured anion and cation concentrations was always less than 10%. Overall, the charge balance errors in the bulk chemical analysis were ≤ 10% for all samples.

Isotopic characterization included determining the deuterium and oxygen isotopic composition of water (δ^2H and δ^{18}O), and the tritium (^{3}H) content. The δ^2H and δ^{18}O were analysed in the University of Malaga using a Wavelength Scanned Cavity Ringdown Spectroscope (WS-CRDS), optimized for isotopic water measurements with a L2120-i Picarro® analyser. For the most saline samples (EC > 12000 µS/cm), δ^{18}O content was analysed in the UB with a Finnigan MAT-253 (Thermo Scientific) Isotope Ratio Mass Spectrometer (IRMS) coupled to an automated line, based on the equilibration between O-water and CO_2 gas following standard methods (Epstein and Mayeda, 1953). The δ^2H content was analysed using a thermo-chemical elemental analyser (TC/EA Thermo-Quest Finnigan) coupled in continuous flow with an IRMS (Thermo Delta XP plus Finnigan Mat). Radioactive isotope H^3 (tritium) content in groundwater was determined by Liquid Scintillation Counting in the ^{14}C and Tritium Dating Service of the Universidad Autónoma de Barcelona. Stable isotope results are expressed in terms of δ per mil relative to the international standards. Reproducibility (1σ) was calculated using international and internal laboratory standards systematically interspersed with the analytical batches: ± 1.0‰ for δ^2H, and ± 0.5‰ for δ^{18}O . Tritium concentrations are expressed as Tritium units (TU) and uncertainty, based on duplicated measurements, is in all cases below 0.2 TU.

Geochemical calculations were carried out with PHREEQC v.3 code (Parkhurst and Appelo 2012) using the Minteq.v4 database supplied with the code.

4. RESULTS AND DISCUSSION

4.1 Structural and geological model

The structural geology of the study area is characterized by a complex interference between several folds systems, displaced by numerous strike-slip and thrust faults (Fig. 2, Fig. 4a).

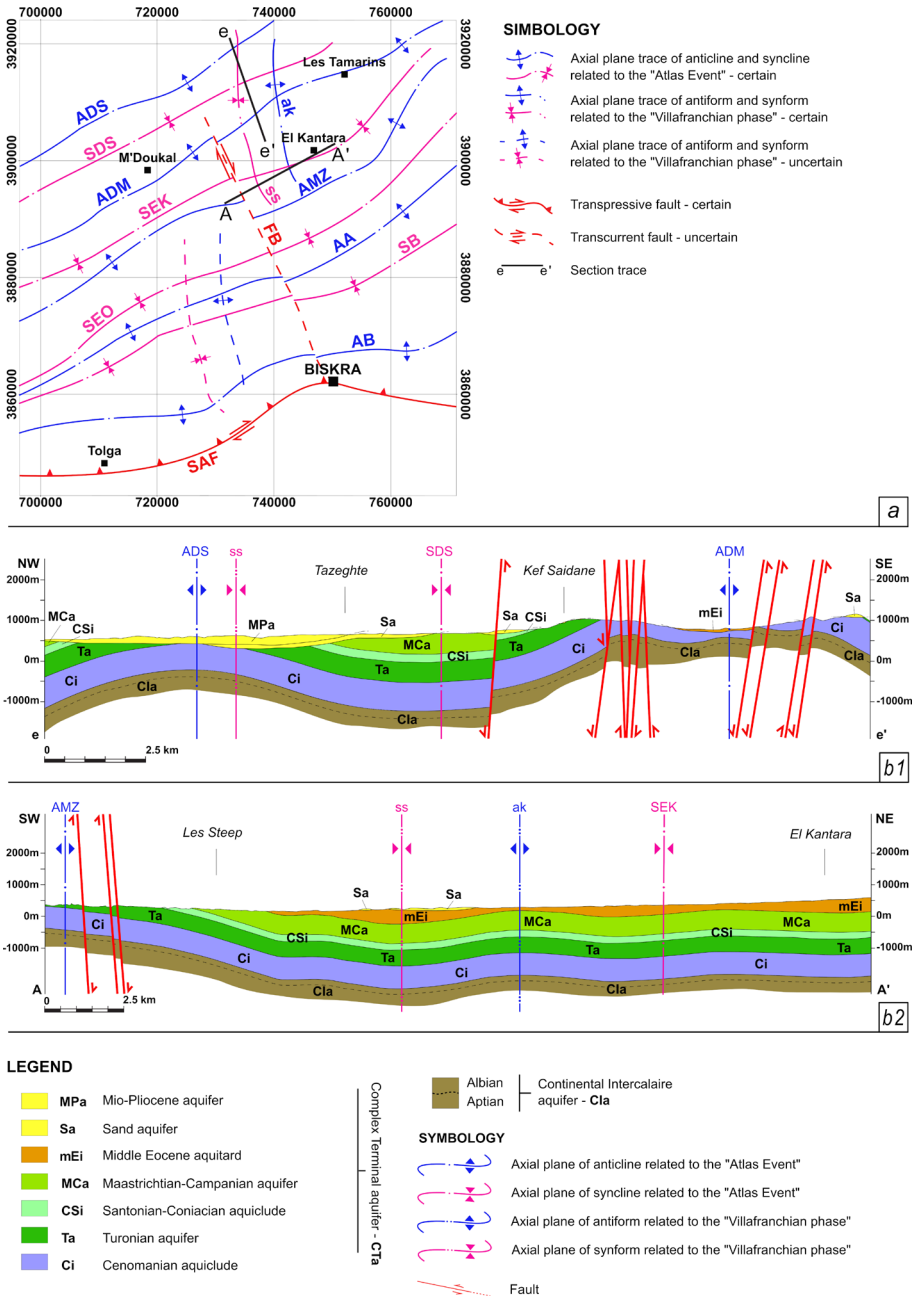

Figure 4 - **a**) Structural sketch map of the region of Biskra; the SAF separates the Saharan Atlas-Aures domain, to the North, from the Sahara Platform to the South; **b**) Representative balanced hydrogeological cross-sections: b1) cross-section e–e' (NW–SE); b2) cross-section A–A' (NE–SW). Douar Sefiane anticline (ADS), Douar Seggana syncline (SDS), Djebel Metlili anticline (ADM), Amentane anticline (AA), Mechtat ez Zmala anticline (AMZ), El Outaya syncline (SEO), Biskra anticline (AB), Branis syncline (SB), El Kantara syncline (SEK), El Kantara antiform (ak), Sefiane synfom (ss), Biskra Fault (FB).

307 The Eocene–Miocene deposits have a maximum thickness in the central part of NE-trending synforms.
308 Their thickness decreases in fold limbs to become discontinuous and disappear on the crests of NE-trending
309 antiforms. This thickness variation does not seemo be related only to erosion, but also in part to
310 progressive deposition of the Miocene succession onto morphological highs that coincide with the crests of
311 the antiforms. The oldest structures recognized are numerous NE-trending folds within the Triassic and
312 Eocene formations: Douar Sefiane anticline (ADS), Douar Seggana syncline (SDS), Djebel Metlili anticline
313 (ADM), El Kantara syncline (SEK), Mechtat ez Zmala anticline (AMZ), El Outaya syncline (SEO), Amentane
314 anticline (AA), Branis syncline (SB), and Biskra anticline (AB) (Fig. 4a).
315 At the cartographic scale, these folds can be considered almost cylindrical, with axes dipping towards the
316 SW and NE. The folds are open and slightly asymmetric (SE-verging), with sub-vertical NE- trending axial
317 planes, a wavelength of about 10 km and an amplitude of about 1.5 km. Discontinuous, lower order folds
318 (wavelength from 10 m to 100 m) are also visible at the cartographic scale, in some lithologies. Initial folds
319 were subsequently deformed by later folding and faulting events. The NE-trending folds are deformed by
320 folds with NW-trending axes dated to the Villafranchian phase. They are discontinuous along axis trend due
321 to interference with the older NE-trending folds, and they are recognizable only at the cartographic scale in
322 the northern sectors of the study area, to the east of Biskra (Figs. 4a, b). These open folds can be
323 considered almost cylindrical, are symmetric with sub-vertical axial planes, and have a wavelength of about
324 5 km and an amplitude of about 500 m. At the map scale, the most recognizable NW-trending folds are the
325 Sefiane synfom (ss) and the El Kantara antiform (ak). Other folds with these trends are thought to be
326 covered by recent deposits. In the study area, numerous normal and reverse faults of variable orientation
327 that displace the oldest fold systems were also mapped (Fig. 2, Figs. 4a and b). The reverse faults are
328 dominant due to their continuity along-strike. They are localized in the flanks of the NE-trending antiforms,
329 but affect only the Mesozoic formations. In some cases, the fault systems are buried by Eocene, Miocene
330 and Quaternary deposits. All of the folds and reverse faults described above are displaced by right lateral
331 strike-slip NNE-striking faults, most visible in the eastern part of the study area. The strike-slip faults offset
332 the axes of the NE-trending folds (Figs. 4a and b). The faults crop out discontinuously because they are

333 often buried by recent Quaternary sediments, but are recognizable by such offsets. The dominant fault
334 (Biskra Fault, FB) in the area of Biskra is a dextral strike slip fault that deforms the AB, the AA and AMZ (Fig.
335 4); its displacement is at least 700 m.
336
337 4.2 *Hydrogeochemistry and Isotopes*
338 The measurements of field parameters as well as the chemical and isotopic results of the water samples
339 from the three field surveys are available as Supplementary data (Tables S1 and S2). A summary statistic
340 (minimum, maximum, mean with standard deviation, and median) of physico-chemical parameters and
341 major ions concentrations for each aquifer is presented in Table 1. Only one water point could be sampled
342 from the AT for analysis of both bulk chemistry and isotope composition, meaning these results could not
343 be extrapolated to the whole of the AT, and are included only as a locally useful observation. In the case of
344 the stable isotopes of water ($\delta^{18}O$ and $\delta^{2}H$), seven additional water points from the AT were sampled,
345 meaning these results could reliably be used to represent the entire aquifer.
346 The limited information available on water point characteristics and well screening hindered the
347 interpretation of results for some samples. Namely, in the case of the samples WA-25 and WA-34, collected
348 at the south of the South Atlas Flexure (SAF in Fig. 2) from the Ta and CIa, respectively, the possibility of
349 water mixing with the overlying aquifers could not be excluded, so there is some uncertainty attached to
350 these data points.

Surface Water/Aquifer	pH					T [ºC]					CE [µS/cm]				
	min	max	mean	SD	median	min	max	mean	SD	median	min	max	mean	SD	median
CIa - Continental Intercalaire (n=6)	6.7	8.1	7.1	0.5	6.9	30	60	43	10	43	3640	14460	7527	5312	4370
Ta - Turonian (n=6)	6.0	8.0	7.3	0.7	7.3	24	30.3	27	2	27	1007	5090	2845	1766	2445
MCa -Maastrichtian-Campanian (n=10)	6.1	8.1	7.3	0.5	7.4	17	25.3	22	3	23	720	4250	1338	1089	933
Lower Eocene- Maastrichtian (n=2)	7.2	7.3	7.3	0.1	7.3	26.2	26.8	27	0	27	1416	1434	1425	13	1425
AT - Lower Eocene (n=1)	-	-	7.2	-	-	-	-	25	-	-	-	-	7440	-	-
MPa - Mio-Pliocene(n=10)	6.8	9.1	7.4	0.6	7.2	21	30.9	24	4	23	1900	7560	4681	2291	4465
Qa - Quaternary (n=17)	7.1	8.8	7.4	0.4	7.3	22	31.5	28	3	29	2590	5660	4096	902	4040
SW - Surface Water (n=5)	6.8	8.7	7.8	0.8	8.0	12.6	28	18	9	13	1917	2900	2429	423	2346

351

Surface Water/Aquifer	Na					Ca					Mg					K				
	min	max	mean	SD	median	min	max	mean	SD	median	min	max	mean	SD	median	min	max	mean	SD	median
CIa - Continental Intercalaire (n=6)	463	2851	1248	1153	527	171	496	349	104	356	49	83	69	16	77	6	84	38	38	25
Ta - Turonian (n=6)	68	711	415	270	463	37	263	125	103	81	26	116	62	42	45	3	11	8	4	10
MCa –Maastricht.-Campanian (n=10)	22	396	94	122	38	50	424	125	107	94	29	147	58	34	50	1	8	3	2	2
Lower Eocene- Maastrichtian (n=2)	79	81	80	1	80	148	157	152	6	152	71	73	72	1	72	4.0	4.0	3.9	0.1	3.9
AT - Lower Eocene (n=1)	-	-	-	973	-	-	-	426	-	-	-	-	225	-	-	-	-	12	-	-

MPa - Mio-Pliocene(n=10)	135	1063	596	382	524	171	439	301	105	290	75	199	122	40	122	2	16	8	5	7
Qa - Quaternary (n=17)	400	859	583	140	597	145	294	198	48	198	63	135	92	24	93	4	12	8	3	8
SW - Surface Water (n=5)	77	252	596	71	209	159	259	222	40	241	32	111	73	29	77	8	10	9	1	9

352

Surface Water/Aquifer	Cl^-					SO_4^{2-}					NO_3^-					HCO_3^-				
	min	max	mean	SD	median	min	max	mean	SD	median	min	max	mean	SD	median	min	max	mean	SD	median
CIa - Continental Intercalaire (n=6)	556	4066	1793	1681	783	631	1622	1176	368	1206	0.5	10.5	3	4	2	147	442	283	116	237
Ta - Turonian (n=6)	78	1017	444	407	272	185	1036	587	377	530	0.7	19.9	8	9	3	240	385	307	63	298
MCa -Maastrichtian-Campanian (n=10)	35	524	122	154	56	45	1419	298	416	149	3.6	13	9	3	10	234	442	315	52	313
Lower Eocene- Maastrichtian (n=2)	85	88	87	2	87	481	482	482	1	482	3.4	3.4	3.4	0.1	3.4	264	266	265	2	265
AT - Lower Eocene (n=1)	-	-	1639	-	-	-	-	1533	-	-	-	-	22.1	-	-	196	-	196	-	-
MPa - Mio-Pliocene(n=10)	178	1710	897	595	871	584	1566	1034	354	1058	7	41.6	19	9	19	232	507	279	84	249
Qa - Quaternary (n=17)	529	1261	834	208	828	548	1183	787	215	807	15.6	33.9	22	7	21	222	347	281	49	258
SW - Surface Water (n=5)	72	377	246	127	273	654	942	791	124	753	0.9	2.9	2.0	1.0	2.5	123	210	157	38	144

353

354 **Table 1** Summary of statistics of physico-chemical parameters and major ions concentration for the surface and groundwater samples collected at the Biskra

355 study area, grouped by aquifer. Concentrations are given in mg/L, SD is the Standard deviation, and “n” indicates the number of samples per aquifer.

356 *4.2.1. Chemical results and Hydrochemical Facies*

357 Temperatures within the Qa and CTa ranged between 21 °C and 29 °C for most samples (Tab. S1), but
358 reached a maximum of 31-32 °C in four sampling points of Qa and one of Ta (WA-25). At least for the
359 samples from the Qa, the majority of the temperatures (27-32 °C) are slightly higher than expected, based
360 on the mean air temperature in the Wilaya Biskra (22 °C) and the geothermal gradient, which is about 4
361 °C/100m (Chenaker et al., 2017). In the CIa, groundwater temperatures range from 41 °C to 60 °C,
362 indicating a geothermal character. According to EC measurements (Tab. S1), only some of the MCa and Ta
363 groundwaters, located in the mountainous northern part of the study area, presents a low level of
364 mineralization, characterized by EC < 1100 µS/cm. In the MCa well located in the plain south of Biskra city
365 (WA-26), where the Maastrichtian is covered by Cenozoic formations, mineralization is greater (EC = 4880
366 µS/cm). All other aquifers as well as the samples WA-26 and WA-25 collected from the MCa and Ta south of
367 the SAF, *i.e.*, where the Upper Cretaceous formations are covered by the Cenozoic formations, present EC
368 ranging from 2000 to 7500 µS/cm. As exception, a maximum of 14400 µS/cm was measured at well WA-18
369 for the thermal groundwater from the CIa. Almost all these EC values are higher than those measured in
370 surface waters (SW), which yield EC values between 1900 and 3000 µS/cm. This indicates that, if SW is
371 recharging the underlying aquifers, it cannot be the only recharge source. Isotopic composition of both
372 surface and groundwater may provide additional insights about the recharge sources (discussed in section
373 4.2.2). The hydrochemical results were plotted on Piper (Fig. 5) and Stiff diagrams (Fig. S2) to allow the
374 differentiation of three main types of waters:

375 Type 1. In the mountainous northern part of the study area, waters with low mineralization of the MCa and
376 Ta (WA-09, WA-31), flowing in limestone formations, are HCO_3 to HCO_3/SO_4 of Ca to Ca/Mg type.
377 Accordingly, these waters are characterized by being mostly equilibrated with calcite and dolomite and
378 subsaturated in gypsum (Fig. 6).

379 Type 2. The surface waters collected from local ephemeral rivers (Oueds) and the Barrage Les Gazelles dam,
380 representing one of the potential sources of recharge for the aquifers in the area, are Ca/Na-SO_4 type. A
381 few samples from the MPa in El Outaya plain (WA-2, WA-13 and WA-24), the CIa (WA-19), and the MCa

382 (WA-08 and WA-26, south of Biskra town), also presented a Ca/Na-SO_4 character. As seen in Fig. 6, they are

383 only slightly saturated in gypsum, in agreement with its Ca/Na-SO_4 character.

384

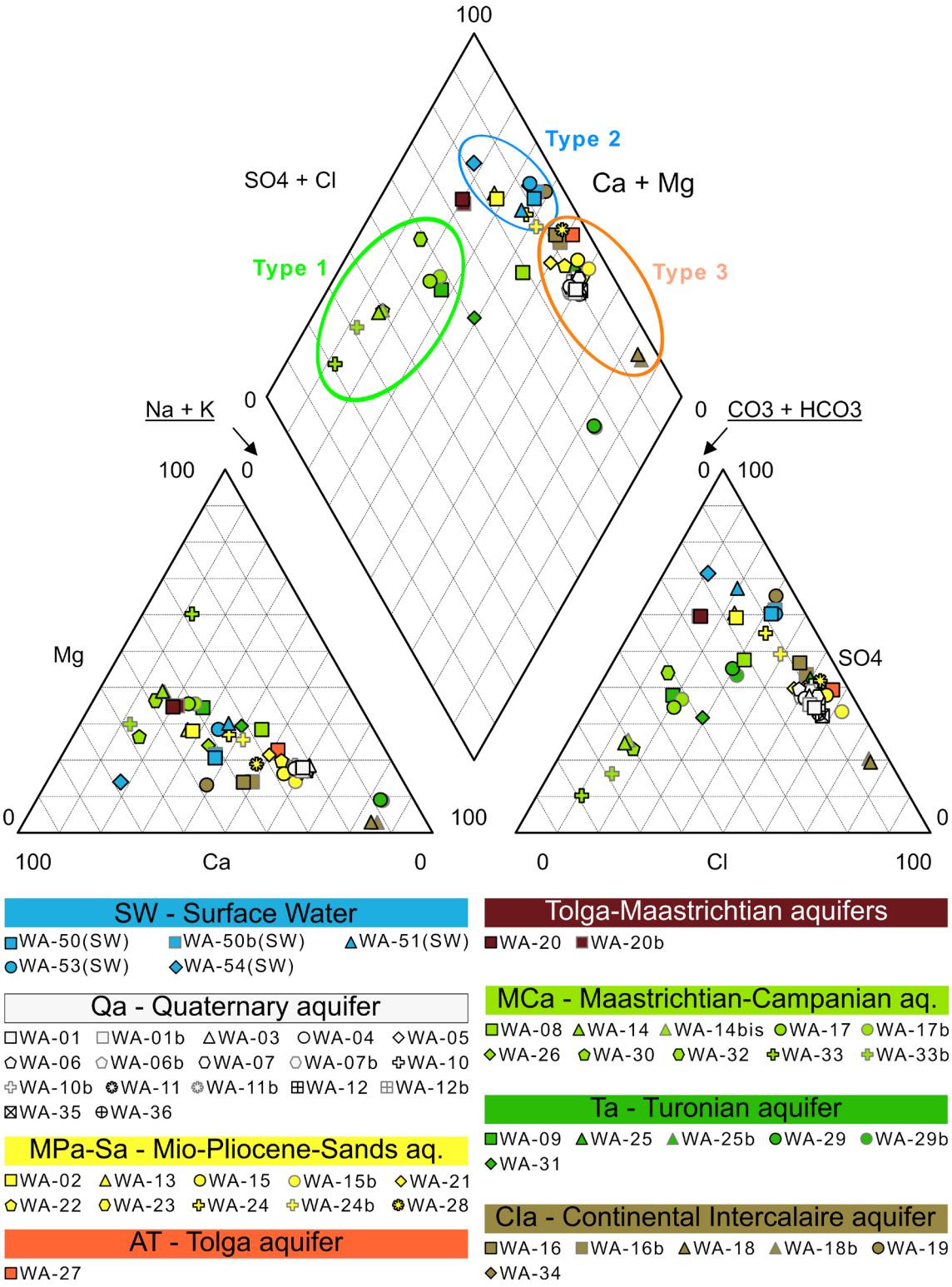

385

386 **Figure 5** - Piper diagram for surface and groundwater samples collected at the Biskra study area, grouped

387 by aquifer.

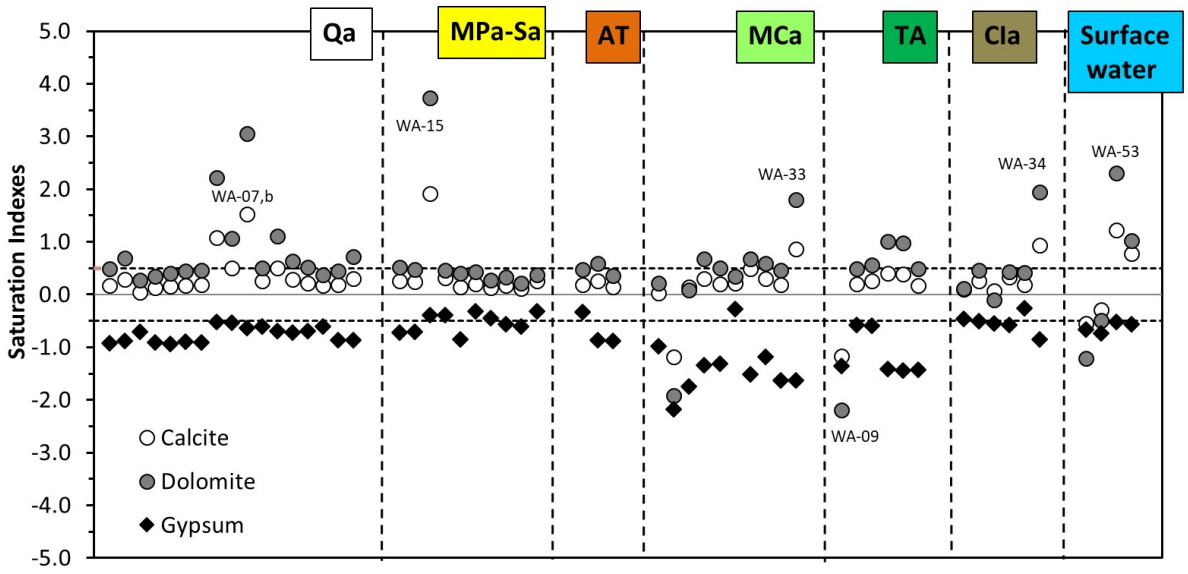

388

389 **Figure 6**. Saturation indexes for calcite, dolomite and gypsum in the water samples compositions listed in

390 table S1.

391

392 Type 3. Groundwater samples from the CIa (WA-16, WA-18 and WA-34), and those from the Cenozoic

393 aquifers (AT, MPa and Qa) collected close to the El Outaya Triassic salt diapir "Djebel El-Melah" (WA-15,

394 WA-28), inside Biskra city and on the plain south of Biskra, present mainly a Na-Cl character, with some

395 tendency toward Cl/SO_4 and Na/Ca type. The CIa groundwater from well WA-18 represents the extreme

396 pole of the group. These results are in line with existing literature. Brinis et al. (2014) found the Neogene

397 groundwaters of El Outaya plain to be of Na-Cl and $Na-SO_4$ type. The samples of Type 3 are in equilibrium

398 with calcite or dolomite and only slightly subsaturated in gypsum (Fig. 6).

399 In all cases, the ratio Na/Cl (in meq/L) is close to 1 (1.2 ± 0.3) suggesting that halite dissolution controls the

400 Na and Cl concentrations in surface and groundwater. Accordingly, all waters are subsaturated in halite (SI

401 < -4, not shown in Fig. 6). Na and Cl concentrations, together with sulphate concentrations are the main

402 contributors to the electrical conductivity of samples.

403

404 *4.2.2 The origin of recharge and aquifer connectivity from water isotopes*

405 The $\delta^{18}O$ and $\delta^{2}H$ results for the water samples collected in the Biskra study area are plotted in Fig. 7,

406 jointly with the Local Meteoric Water Line (LMWL, $\delta^{2}H = 7.2\ \delta^{18}O + 8$. Correlation coefficient R^2=0.92) and

the weighted mean value for modern rainfall (-5.9 ± 2.6‰ for $\delta^{18}O$ and -39 ± 19‰ for $\delta^{2}H$). The two latter have been obtained by using the data available at the Global Network of Isotopes in Precipitation (GNIP. IAEA/WMO, 2020) for the station of Algiers University from 2000 to 2003 (n=75). The LMWL obtained with such data is similar to that found in literature (Saighi, 2005. $\delta^{2}H = 7.15\ \delta^{18}O + 7.92$, R^2=0.92, n=113). Fig. 7 shows that for surface waters the $\delta^{18}O$ values range from -0.1‰ to -6.5‰, and the $\delta^{2}H$ values from -9‰ to -45‰. Isotopic composition of the surface waters collected from the *Barrage Fontaine des Gazelles* at two different times (WA-50 and WA-50b) is likely the result of evaporation processes from the same source (*i.e.*, reservoir effect). An evaporation line of $\delta^{2}H = 3.9\ \delta^{18}O - 9$ was estimated (Fig. 7). The slope of the obtained evaporation line is similar to that (4.6) reported by Fontes and Gonfiantini (1967) for two seasonal lakes (Sebkha el Melah and Gara Diba Guelta) located in northwestern Sahara. The isotopic composition of the rest of the surface water samples was fitted to an evaporation line with this 3.9 slope (Fig. 7) and the intersection of this evaporation line with the LMWL would indicate the isotopic signature of local precipitation in the northern mountainous area of El Kantara. Surface water from WA-129 is thus likely representing aquifer recharge in the El Kantara area.. The groundwater samples are mostly distributed along the LMWL, with $\delta^{18}O$ ranging from -4.0‰ to -8.8‰, and $\delta^{2}H$ from -29‰ to -59‰ (Tabs. S1 and S2). Four main groups can be identified within the isotope data, from lightest to heaviest, which depict the evolution of groundwater and mixing between different aquifers of the study area (more detail can be found in section 4.3).

Group 1. The first group includes samples from the Cla, and those from the Ta collected in the mountainous northern areas (Daira of El Kantara and Djamourah), with $\delta^{18}O$ around -8.4‰ and $\delta^{2}H$ between -55‰ and -59‰. This group corresponds to the lower stratigraphic formations, despite the Turonian formation is partially outcropping in this area. Similar depleted values were already found in the deep groundwater of the Hodna region (Gonfiantini et al., 1974), to the north of the study area. Obtained isotopic composition for Cla samples is consistent with the ranges ($\delta^{18}O$ between -8‰ and -9‰ and $\delta^{2}H$ between -55‰ and -70‰) reported previously for deep Cla groundwaters (Abdelali et al., 2020; Edmunds et al., 2003; Moulla et

al., 2002). Similar values were also found in two hot springs from the Biskra area ($\delta^{18}O$ between -7.7‰ and -8.8‰ and $\delta^{2}H$ between -55‰ and -62‰, Chenaker et al., 2017).

Group 2. The second group is mainly made up of the MCa waters with low mineralization, which have $\delta^{18}O$ and $\delta^{2}H$ around -7.8‰ and -51‰, respectively. These water points are located in the mountainous area of El Kantara and Djamourah, where the Maastrichtian formations crop out. In addition, sample WA-21 from the MPa, located near Biskra town, also belongs to Group 2. Its $\delta^{18}O$ and $\delta^{2}H$ composition is intermediate between the CIa water of Group 1 and the remaining MPa waters of Group 3 (see next paragraph), which points to the ascension of depleted CIa groundwater in the south part of the study area, affecting the isotopic composition of water in the overlying aquifers. These mixing processes are also supported by the Cl *vs* $\delta^{2}H$ plot (Fig. S3). Chemical and isotopic composition of the low mineralized MCa waters belonging to this Group 2 (variable Cl content but narrow $\delta^{2}H$ range) is likely the result of water-rock interaction.

Group 3. Consistent with their similarities in bulk chemistry, the waters from the Qa, MPa and AT show similar ^{2}H and ^{18}O isotopic compositions ($\delta^{18}O$ ranging from -6.6‰ to -7.4‰, and $\delta^{2}H$ from -44‰ to -50‰), constituting a third main group of waters and revealing a connection among these aquifers in the study area. Some of the MCa, Ta (WA-25) and CIa (WA-34) samples also belong to Group 3. These samples were collected at the south of the SAF where, contrary to other parts in the north, the Upper Cretaceous formations are covered by Cenozoic formations. A mixing of water from different aquifers due to poor screening of the wells cannot be excluded for the point WA-25. A mixing of ascending thermal water (CIa) with different waters from the aquifers intersected during ascent can explain the hydrochemical and isotopic characteristics of the spring sample WA-34. The plot Cl vs $\delta^{2}H$ (Fig. S3) also supports this hypothesis. The raise up of thermal waters through deep-seated faults acting as hydrothermal conduits has already been suggested for this area (Chenaker et al., 2017). Chemical and isotopic data also suggest that most of the samples from Group 3 have a significant contribution from saline CIa waters (Fig. S3).

Group 4. Finally, a fourth group could also be identified, composed of MPa water samples showing a heavier isotopic composition with respect to those of Group 3, with $\delta^{18}O$ and $\delta^{2}H$ values of up to -4‰ and -29‰ respectively. This isotopic composition suggests the MPa aquifer is likely receiving a locally important

recharge contribution from evaporated surface waters in the corresponding sampled areas or that some degree of evaporation of precipitation occurred prior to infiltration. Tritium content for sample WA-15, collected close to Oued El Hai Biskra, supports this hypothesis in El Outaya Plain (see in the following).

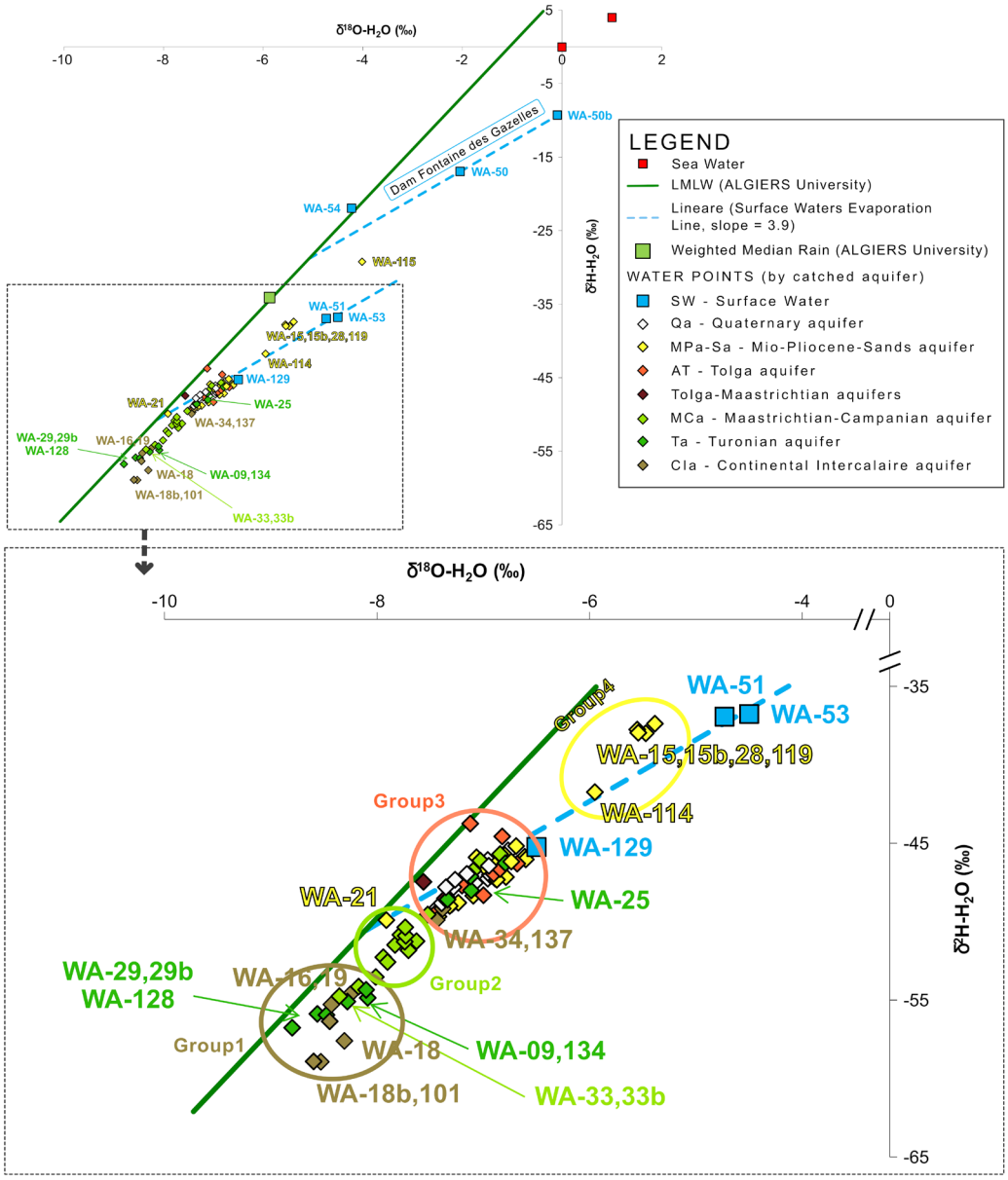

Figure 7 – $\delta^{18}O$ vs. $\delta^{2}H$ plot for water samples collected at the Biskra study area. Diamonds are representative of groundwater samples and are coloured according to the aquifer they were collected from, with reference to the legend in Fig. 2. The blue square symbols represent surface water samples. The zoomed part of the plot allows the reader to better distinguish the four identified water groups.

467 The content of Tritium in all the sampled waters ranged from 0 to 3.5 TU (Tab. S1). Considering the most
468 recent data for Tritium in precipitation close to the study area (GNIP, IAEA/WMO, 2020. Data from Algiers-
469 CN station, year 2004, n=3, average Tritium value = 6.9 TU) and the Tritium semidecay period of 12.5 years,
470 an approximate content of 4 TU could be expected for actual precipitation in the sampling period (years
471 2012-2014) at the Biskra and Batna region. The value of 3.5 TU found for surface waters in the study area
472 (sample WA-54) is in agreement with such estimate. It thus corresponds to the isotopic signal of actual
473 precipitation and suggests that surface waters in the sampled area are not receiving any contribution from
474 the underlying aquifers. The Tritium content in the CIa groundwater (0–0.4 TU) indicates this aquifer was
475 recharged more than 60 years ago ("pre-bomb" waters). The remaining groundwaters are mainly
476 characterized by Tritium values between 0.4 and 1.5 TU, with a maximum of 3.1 TU observed in the MPa
477 sample WA-15. Again, these findings give support to the hypothesis of CTa and even Qa waters to be a
478 mixture between pre-atomic-bomb (> 60 years) water and recent surface waters. This mixing process has
479 been previously demonstrated for CIa (insignificant Tritium content) and CTa groundwater (up to 4.8 TU) in
480 the Ouargla area (Guendouz et al., 2006; Moulla et al., 2002).
481
482 *4.3 The 3D hydrogeological conceptual model*
483 Fig. 8 shows the 3D hydrogeological conceptual model of the Biskra and Batna region, obtained integrating
484 geological, structural, well logs from the literature (*i.e.*, permeability, saturated thickness, specific yield),
485 hydrochemical and isotopic data.
486 The reconstruction of the structural setting shows that the hydrogeological basin has a complex geometry,
487 which affects groundwater flow. Geometries of the aquifers are strongly influenced by the deformation
488 history of the Mesozoic and Eocene rocks, which is related to the building of the Atlas Mountains.
489 Moreover, the presence of faulting, which brought impermeable and permeable layers into contact, has
490 likely created a preferential pathway for deep water to ascend into upper aquifers, as indicated by
491 hydrogeochemical and isotopic data, as detailed as follows. First, the distribution of groundwater
492 temperatures suggests a potential contribution of thermal deep waters (CIa) to the overlying aquifers, since

493 the majority of temperatures at least within the Qa (27-32 °C, Table S1) are slightly higher than expected on
494 the base of the mean air temperature in the Wilaya Biskra (22 °C) and the geothermal gradient, which is
495 about 4.1 °C/100m (Chenaker et al., 2017). Second, the deepest groundwaters, from the CIa, are the
496 isotopically lightest ($\delta^{18}O$ around -8.4‰ and $\delta^{2}H$ between -55‰ and -59‰; Group 1 in section 4.2.2), in
497 accordance with previous authors, who, with additional supporting evidence from $\delta^{13}C$ and ^{14}C isotopic
498 analyses, attributed this depleted signature to a recharge event that occurred during a cooler climatic
499 regime at the end of Pleistocene (Edmunds et al., 2003; Guendouz et al., 2003). The Ta samples collected in
500 the northern mountainous area where the Turonian formations crops out are expected to be influenced by
501 local precipitation and therefore to be similar to samples from Group 2 (described in section 4.2.2.).
502 Nevertheless, they present a depleted signature that could be typically characteristic of the Turonian
503 groundwater, or could be explained by some ascension and mixing with CIa water too. Third, the higher
504 electrical conductivity values of the Cenozoic groundwaters (Qa, MPa and AT), compared with those of
505 surface waters, and their hydrochemical character, suggest an intense interaction of these groundwaters
506 with the formations they flow through, or a potential contribution from deeper CIa water migrating
507 through the fault network. Finally, the variability in Tritium concentration in groundwater within the same
508 aquifer (except those from CIa) could indicate mixing in different proportions (and different transit times)
509 of pre-atomic-bomb (> 60 years) and recent waters. In the case of Qa, according to a study based on
510 piezometric head variations corresponding to floods events during two-year observations (SCET-COOP
511 1967), recharge by direct infiltration from floods cannot be discarded. Nevertheless, the Tritium results for
512 this aquifer (0.4 TU to 1 TU) compared with the Tritium content measured in local surface waters (3.5 UT
513 for sample WA-54) and the value estimated for actual precipitation in the region (about 4 UT, based on
514 GNIP IAEA/WMP 2020 data, as commented in section 4.2.2) suggest that the Qa receives a small recharge
515 of surface water (consistent with the low precipitation regime and intense flood events characteristic of the
516 area), along with a contribution from Cretaceous aquifers. All these hydrochemical and isotopic data
517 therefore suggest that the chemical and isotopic composition of the Cenozoic groundwater is possibly a
518 result of the mixing between three end-members: current water recharge (*i.e.*, precipitation + surface

519 water/runoff in El Kantara and El Outaya/Biskra Plain), deep saline CIa groundwater and non-saline
520 Cretaceous (CIa, MCa and Ta) groundwater (Fig. 7, Fig. S3). This type of mixing would again support the
521 hypothesis on the influence of the existing fault network on the hydrogeochemistry of the study area.
522 Shortening related to Upper Cretaceous deformation was accommodated by folds, causing the thickening
523 of cover and, consequently, of the aquifers. These folds constitute structural highs that can play an
524 important role in recharging or dispersing surface water flows. Moreover, crests of the major antiforms
525 often set up the watershed boundaries and, in the northern part of the study area, can constitute recharge
526 areas for the Upper Cretaceous aquifers. According to the $\delta^{18}O$ and $\delta^{2}H$ results, the recharge of the low
527 mineralized MCa waters (Group 2 in Fig. 7) could mainly be influenced by local precipitation and runoff in
528 the El Kantara and Djamourah mountainous areas (sample WA-129 in Fig. 7). The Tritium content (0.6 – 1.7
529 TU) jointly with the low salinity (EC < 2000 µs/cm) and bulk chemistry of the MCa waters, jointly with its
530 isotopic composition (Fig. S3), suggest they are a mix of pre-bomb (deeper flow-lines within the MCa
531 aquifer) and recent water, but they are not affected by contributions from the deepest CIa groundwaters.
532 Antiforms can strongly influence the groundwater flow direction by forcing the flow towards the synformal
533 axis. The most prominent synclines are SDS, SEK, SEO and SB (Fig. 2; Figs. 4a, b; Fig. 8). They could act as
534 storage areas allowing the accumulation of huge reserves of groundwater. Locally, synform geometries
535 involving marl strata can allow the formation of perched aquifers.
536 In the area of El Kantara (Fig. 2; Figs. 4a, b), ss and the ak are superimposed on the ADM and SEK. The
537 superposition of folds with different trends can lead to very complex structures. In this specific case, the
538 type of interference is known as 'dome and basin' (Type I, Ramsay, 1967), and such a pattern produces
539 zones of water accumulation that should heavily impact on the groundwater contributions.
540 The carbonate rocks constituting the Mesozoic and Eocene aquifers have a geometry related to the NE-
541 trending fold systems and a regional dip that forces groundwater to flow towards the SSW (Fig. 8). NW–SE
542 trending faults like the strike-slip FB complicate the model of the groundwater circulation (Fig. 8). The
543 effects of the existing fault network on the hydrogeology of the study area can be summarized as: i) Fault
544 displacement allows interconnection between aquifers separated by low permeability formations, as in the

case of the connection between the Ta and the MCa; ii) Fault structure diverts part of the SSW groundwater flow toward an NW-SE direction; iii) Fault planes act as the preferred path for the rise of deep (Cretaceous) groundwaters, even the thermal waters from CIa, which supply the shallow aquifers MPa and Qa. The occurrence of this mixing was supported by groundwater temperature data, bulk chemistry and isotopic results.

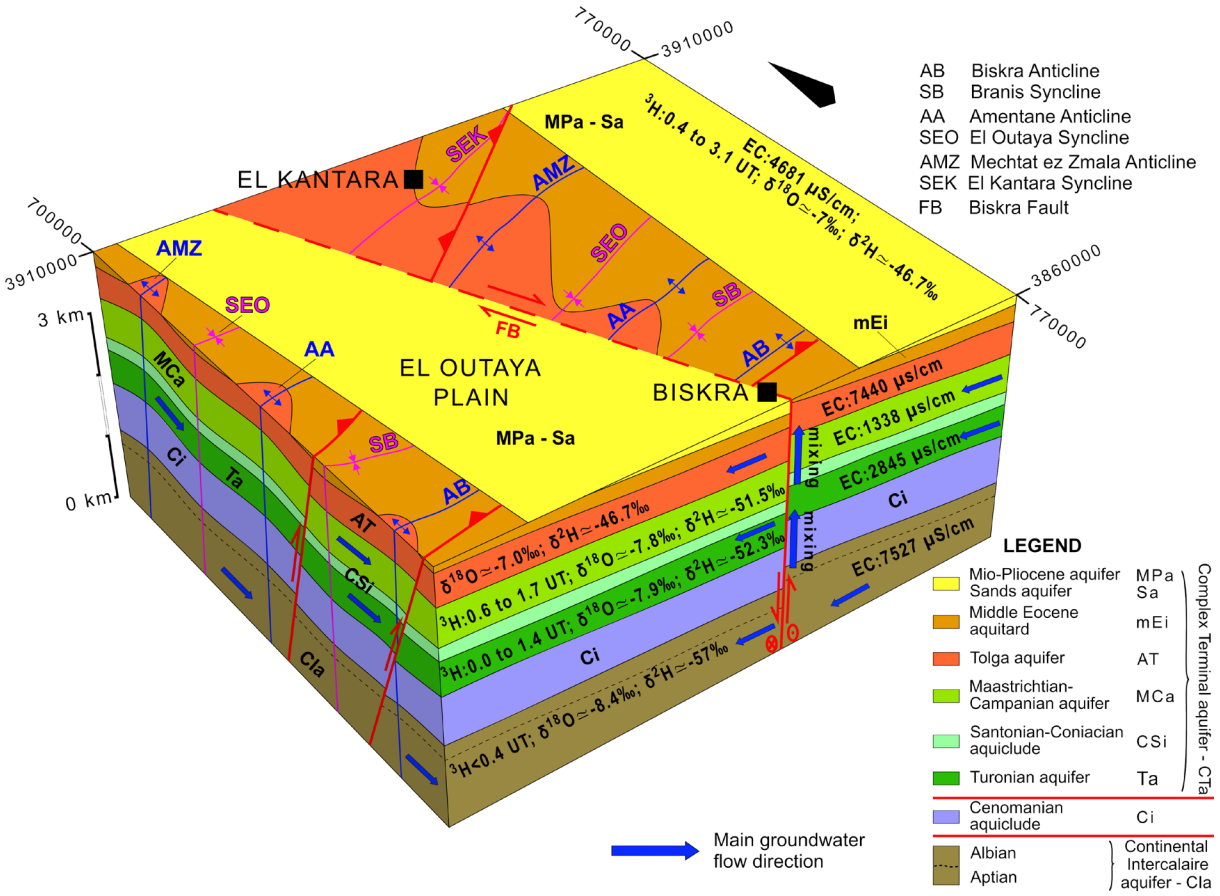

Figure 8 - 3D hydrogeological conceptual model.

5. CONCLUSION

In this paper, a methodological approach to construct a 3D hydrogeological conceptual model of complex aquifers systems with high hydrogeological heterogeneity has been elaborated and applied to the Biskra and Batna region. The conceptual model obtained, based on the reconstruction of a 3D geological model, combined with existing hydrogeological information, data points from new hydrogeological field surveys, and hydrogeochemical and isotope data from selected sampling points, allows the full 3D geometries of the aquifers to be reconstructed; this is impossible to be done through simple correlation of layers identified in

560 stratigraphic logs. The model sheds light on the physical limits of the aquifer units (as close to reality as
561 possible, based on available data) existing in the study area, as well as on recharge and discharge areas, and
562 groundwater flow directions. The conceptual model can be used directly in numerical flow modelling in the
563 next stages of investigation, and also provides an insight into the vulnerability of the aquifers to potential
564 anthropogenic pollution phenomena.
565 The results of this study show the important role that tectonic settings can play in the hydrogeology and
566 hydrochemistry of primary groundwater systems. The southern part of the study area, nearby Biskra city, is
567 most affected by geological structures. The fault network connects different aquifers resulting in the mixing
568 of groundwaters. Besides a limited contribution of surface water recharge from flood events, the recharge
569 of the Cenozoic aquifers seems to proceed by the ascendance of deep Cretaceous groundwaters through
570 the fault network, as indicated by temperature, bulk chemistry and isotopic (in particular, Tritium) data.
571 Aquifer interconnection induced by fault systems represents a concern for groundwater quality. Indeed,
572 the Cla waters are hot and highly mineralized. Their contribution to the recharge of the Cenozoic aquifers,
573 heavily exploited for domestic and irrigation use, may diminish their quality. This example shows how
574 improved knowledge of fault networks gathered by the use of 3D geological models coupled with the
575 hydrogeochemical/isotopic data from aquifers can be a powerful tool to understand the main factors that
576 control water resources quality and their vulnerability to contamination. The proposed approach may be
577 useful for the characterization of water resources in arid areas where environmental conditions and
578 political context prevent extensive field characterization. The information that a 3D understanding of the
579 complexity of the underground systems can yield may be crucial in informing the design and
580 implementation of efficient strategies aimed at improving the management of water resources, and the
581 protection of their quality. The implementation of MAR (Managed Aquifer Recharge) systems promoted by
582 the WADIS-MAR Project would increase the contribution of fresh surface water from floods to the recharge
583 of shallower aquifers, thus improving their water quality and allowing more efficient management of the
584 available water resources. Once 3D-geological models have been constructed, the ability to manage geo-
585 objects with spatial variations in their properties can be exploited by planners, engineers, geotechnical

586 engineers, and developers to perform quantitative spatial analysis and a range of other professional
587 applications (Butscher et al., 2017; Zhu et al., 2013).
588
589 **Acknowledgments**
590 This study was funded by the European Union in the frame of the WADIS-MAR project (www.wadismar.eu),
591 Grant Contract ENPI/2011/280-008, led by the University of Sassari (Italy) and coordinated by Giorgio
592 Ghiglieri, and partially by the project 2017SGR1733 from the Catalan Government (Generalitat de
593 Catalunya). This is one of the five Demonstration Projects implemented within the Regional Programme
594 "Sustainable Water Integrated Management (SWIM)" (www.swim-sm.eu). We are grateful to Midland
595 Valley Exploration Ltd. for providing an academic license for the use of Move software.
596
597 **Supplementary data**
598 Supplementary data to this article can be found online at https://doi.org/10.1016/j.scitotenv.2020.143797.
599
600 **REFERENCES**
601 Abdelali, A., Nezli, I. E., Kechiched, R., Attalah, S., Benhamida, S. A., & Pang, Z., 2020. Geothermometry and
602 geochemistry of groundwater in the Continental Intercalaire aquifer, southeastern Algeria: Insights from
603 cations, silica and SO4–H2O isotope geothermometers. Applied Geochemistry, 113, 104492.
604 https://doi.org/10.1016/j.apgeochem.2019.104492
605 Afrasinei, G. M., Melis, M. T., Buttau, C., Bradd, J. M., Arras, C., & Ghiglieri, G., 2015. Diachronic analysis of
606 salt-affected areas using remote sensing techniques: the case study of Biskra area, Algeria. Proceedings of
607 SPIE, 9644, 96441D. https://doi.org/http://dx.doi.org/10.1117/12.2194998
608 Afrasinei, G. M., Melis, M. T., Buttau, C., Bradd, J. M., Arras, C., & Ghiglieri, G., 2017. Assessment of remote
609 sensing-based classification methods for change detection of salt-affected areas (Biskra area, Algeria).
610 Journal of Applied Remote Sensing, 11(1), 016025. https://doi.org/10.1117/1.JRS.11.016025

American Public Health Association (APHA), American Water Works Association (AWWA), and Water Environment Federation (WEF), 1998. Standard Methods for the Examination of Water and Wastewater 20th Edition. United Book Press, Inc., Baltimore, Maryland

Arras, C., Melis, M. T., Afrasinei, G.-M., Buttau, C., Carletti, A., & Ghiglieri, G., 2017. Evaluation and validation of SRTMGL1 and ASTER GDEM2 for two Maghreb regions (Biskra, Algeria and Medenine, Tunisia). In M. Ouessar, D. Gabriels, A. Tsunekawa, & S. Evett (Eds.), Water and Land Security in Drylands: Response to Climate Change (pp. 291–301). Springer. https://doi.org/10.1007/978-3-319-54021-4_24

Beck, H., Zimmermann, N., McVicar, T., Vergopolan, N., Berg, A., Wood, E., 2018. Present and future Köppen-Geiger climate classification maps at 1-km resolution. Sci Data 5, 180214. https://doi.org/10.1038/sdata.2018.214 .

Biddau, R., Cidu, R., Da Pelo, S., Carletti, A., Ghiglieri, G., Pittalis, D., 2019. Source and fate of nitrate in contaminated groundwater systems: Assessing spatial and temporal variations by hydrogeochemistry and multiple stable isotope tools. Science of the Total Environment, 647, pp. 1121-1136. https://DOI.10.1016/j.scitotenv.2018.08.007.

Bracène R, Frizon de Lamotte D., 2002. The origin of intraplate deformation in the Atlas system of western and central Algeria: From Jurassic rifting to Cenozoic-Quaternary inversion. Tectonophysics 357:207–226, https://doi.org/10.1016/S0040-1951(02)00369-4.

Bracène R., Patriat M., Ellouz N., Gaulier J.N., 2002. Subsidence history in basins of northern Algeria. Sedimentary Geology, 156(1), 213-239, https://doi.org/10.1016/S0037-0738(02)00289-0.

Brinis, N., Boudoukha, A., Djaiz, F. 2014. Case of aquifer of El-Outaya. North-west of Biskra – ALGERIA. International Journal of Environment & Water, Vol.3, Issue 1. ISSN 2052-3408.

Butscher C., Scheidler S., Farhadian H., Dresmann H., Huggenberger P., 2017. Swelling potential of clay-sulfate rocks in tunneling in complex geological settings and impact of hydraulic measures assessed by 3D groundwater modeling. Eng. Geol. 221, 143-153, https://doi.org/10.1016/j.enggeo.2017.03.010.

635 Chenaker, H., Houha, B., Valles, V., 2017. Isotope studies and chemical investigations of hot springs from
636 North-Eastern Algeria. J. Mater. Environ. Sci, 8(12), 4253-4263,
637 http://www.jmaterenvironsci.com/Document/vol8/vol8_N12/448-JMES-3204-Chenaker.pdf.
638 Colombani, N., Mastrocicco, M., Castaldelli, G., Aravena, R., 2019. Contrasting biogeochemical processes
639 revealed by stable isotopes of H2O, N, C and S in shallow aquifers underlying agricultural lowlands.
640 Science of the Total Environment, 691, pp. 1282-1296. https://DOI.10.1016/j.scitotenv.2019.07.238.
641 Da Pelo S, Ghiglieri G, Buttau C, Biddau R, Cuzzocrea C, Funedda A, Carletti A, Vacca S, Cidu R., 2017.
642 Coupling 3D hydrogeological modelling and geochemical mapping for an innovative approach to support
643 management of aquifers. Ital. J. Eng. Geol. Environ. 41–51. https://doi.org/10.4408/IJEGE.2017-01.S-04 .
644 de Jong C., Cappy S., Finckh M., Funk D., 2008. A transdisciplinary analysis of water problems in the
645 mountainous karst areas of Morocco. Eng. Geol. 99 (3–4), 228-238,
646 https://doi.org/10.1016/j.enggeo.2007.11.021.
647 Edmunds, W.M., Guendouz, A., Mamou, A., Moulla, A., Shand, P., Zouari, K., 2003. Groundwater evolution
648 in the Continental Intercalaire aquifer of Southern Algeria and Tunisia: trace element and isotopic
649 indicators. Appl. Geochem. 18, 805–822, https://doi.org/10.1016/S0883-2927(02)00189-0 .
650 Epstein S., Mayeda T., 1953. Variation of O18 content of waters from natural sources. Geochimica et
651 Cosmochimica Acta, Volume 4, Issue 5, Pages 213-224, ISSN 0016-7037, https://doi.org/10.1016/0016-
652 7037(53)90051-9.
653 Fontes, J.C., Gonfiantini, R., 1967. Comportement isotopique au cours de l'évaporation de deux bassins
654 sahariens. Earth and Planetary Science Letters, 3, 258-266, https://doi.org/10.1016/0012-821X(67)90046-
655 5
656 Frizon de Lamotte D., Saint Bezar B., Bracène R., Mercier E., 2000. The two main steps of the atlas building
657 and geodynamics of the west Mediterranean. Tectonics 19 (4), 740– 761.
658 Gamboa C., Godfrey L., Herrera C., Custodio E., Soler A., 2019. The origin of solutes in groundwater in a
659 hyper-arid environment: A chemical and multi-isotope approach in the Atacama Desert, Chile. Sci. Total
660 Environ. 686, pp. 709-718. https://doi.org/10.1016/j.scitotenv.2019.06.356.

661 Ghiglieri G., Carletti, A., 2010. Integrated approach to choosing suitable areas for the realization of
662 productive wells in rural areas of Sub-Saharan Africa (southern Hodh El Chargui, Mauritania SE)" - Hydrol.
663 Sci. J. 55(8), 1357- 1370. Taylor & Francis ISSN 0262-6667 -
664 https://doi.org/10.1080/02626667.2010.527845.
665 Ghiglieri G., Baba Sy M.O., Yahyaou H., Ouessar M., Ouldamara A., Soler I Gi A., Arras C., Barbieri M.,
666 Belkheiri O., Zaied M.B., Buttau C., Carletti A., Da Pelo S., Dodo D., Funedda A., Iocola I, Meftah E., Mokh
667 F., Nagaz K., Melis M.T., Pittalis D., Said M., Sghaier M., Torrentó C., Virdis S., Zahrouna A., Enne G., 2014.
668 Design of artificial aquifer recharge systems in dry regions of Maghreb (North Africa). Flowpath 2014 –
669 National Meeting on Hydrogeology, 144-145, ISBN 978-88-907553-4-7 -
670 https://doi.org/10.13140/2.1.1710.1764.
671 Ghiglieri, G., Carletti, A., Da Pelo, S., Cocco, F., Funedda, A., Loi, A., Manta, F., Pittalis, D., 2016. Three-
672 dimensional hydrogeological reconstruction based on geological depositional model: A case study from
673 the coastal plain of Arborea (Sardinia, Italy). Eng. Geol., 207, 103-114.
674 https://doi.org/10.1016/j.enggeo.2016.04.014.
675 Gonfiantini, R., Dincer, T., Derekoy, A. M., 1974. Environmental isotope hydrology in the Hodna region,
676 Algeria. In: Isotope techniques in groundwater hydrology 1974, Vol. I. Proceedings of a symposium, pp.:
677 293-316.
678 Guendouz A., Moulla A. S., Edmunds W.M., Zouari K., Shand P., Mamou A., 2003. Hydrogeochemical and
679 isotopic evolution of water in the Complexe Terminal aquifer in the Algerian Sahara. Hydrogeology
680 Journal, 11, 483–495, https://doi.org/10.1007/s10040-003-0263-7 .
681 Guendouz, A., Moulla, A. S., Remini, B., Michelot, J. L. 2006. Hydrochemical and isotopic behaviour of a
682 Saharan phreatic aquifer suffering severe natural and anthropic constraints (case of Oued-Souf region,
683 Algeria). Hydrogeology Journal, 14, 955-968, https://doi.org/10.1007/s10040-005-0020-1.
684 Guiraud R., Bosworth W., 1997. Senonian basin inversion and rejuvenation of rifting in Africa and Arabia:
685 synthesis and implications to plate-scale tectonics. Tectonophysics 282:39–82.
686 http://dx.doi.org/10.1016/S0040-1951(97)00212-6

687 IAEA/WMO, 2020. Global Network of Isotopes in Precipitation. The GNIP Database. Accessible at:
688 https://nucleus.iaea.org/wiser
689 MdH, Ministere de l'Hidraulique Algerienne, 1980. - Direction des Etudes de Milieu et de la Recherche
690 Hydraulique, Service Hydrogeologie, Clairbois, Birmanreis, Alger. Notice explicative de la Carte
691 Hydrogeologique de Biskra au 1/200000.
692 Moulla A.S, Guendouz A , Cherchali MEH, 2002. Contribution des isotopes à l'étude des ressources en eau
693 souterraines transfrontalières en Algérie. Proceedings of the international workshop. Tripoli, Libya.
694 Palmer, P.C.; Gannett, M.W.; Hinkle, S.R., 2007. Isotopic characterization of three groundwater recharge
695 sources and inferences for selected aquifers in the upper Klamath Basin of Oregon and California, USA. J.
696 Hydrol. 336, 17-29, https://doi.org/10.1016/j.jhydrol.2006.12.008.
697 Parkhurst, DL, Appelo, CAJ (2012) Description of input and examples for PHREEQC version 3—a computer
698 program for speciation, batch-reaction, one-dimensional transport, and inverse geochemical calculations.
699 USGS Techniques and Methods, book 6, chap. A43, 497 p., available only at http://pubs.usgs.gov/tm/06
700 A43/.
701 Pittalis, D., Carrey, R., da Pelo, S., Carletti, A., Biddau, R., Cidu, R., Celico, F., Soler, A., Ghiglieri, G., 2018.
702 Hydrogeological and multi-isotopic approach to define nitrate pollution and denitrification processes in a
703 coastal aquifer (Sardinia, Italy). Hydrogeology Journal, Volume II pages 1-20.
704 https://doi.org/10.1007/s10040-018-1720-7.
705 Puig, R., Soler, A., Widory, D., Mas-Pla, J., Domènech, C., Otero, N., 2017. Characterizing sources and
706 natural attenuation of nitrate contamination in the Baix Ter aquifer system (NE Spain) using a multi-
707 isotope approach. Sci. Total Environ. 580, 518–532. https://DOI.10.1016/j.scitotenv.2016.11.206 .
708 Ramsay, J. G., 1967. Folding and fracturing of rocks. Mc Graw Hill Book Company 568.
709 Ross M., Parent M. & Lefebvre R., 2005. 3D geologic framework models for regional hydrogeology and
710 land-use management: a case study from a Quaternary basin of southwestern Quebec. Canada.
711 Hydrogeology Journal, 13, 690–707. https://doi.org/10.1007/s10040-004-0365-x.

712 Saighi, O. 2005. Isotopic composition of precipitation from Algiers and Assekrem. In: Isotopic composition
713 of precipitation in the Mediterranean Basin in relation to air circulation patterns and climate. IAEA-
714 TECDOC-1453, Isotope Hydrology Section. Vienna, Austria, 5-17
715 SCET-COOP, 1967. Oued Biskra: Eaux souterraines - Etude des ressources exploitables sur analyseur
716 électrique a réseau r.c.
717 Touch S., Likitlersuang S., Pipatpongsa T., 2014. 3D geological modelling and geotechnical characteristics of
718 Phnom Penh subsoils in Cambodia. Eng. Geol. 178, 58-69, https://doi.org/10.1016/j.enggeo.2014.06.010.
719 Tullen, P., Turberg, P., Parriaux, A., 2006. Radiomagnetotelluricmapping, groundwater numerical modelling
720 and 18O-oxygen isotopic data as combined tools to determine the hydrogeological system of a landslide
721 prone area. Eng. Geol. 87 (3–4), 195–204. https://doi.org/10.1016/j.enggeo.2006.07.004.
722 www.mve.com/software/move.
723 www.swim-sm.eu.
724 www.wadismar.eu.
725 Xue, Y., Sun, M., Ma, A., 2004. On the reconstruction of three-dimensional complex geological objects using
726 Delaunay triangulation. Futur. Gener. Comput. Syst. 20, 1227–1234.
727 https://doi.org/10.1016/j.future.2003.11.012.
728 Zhu, L., Li, M., Li, Chang-ling, Shang, J., Chen, G., Zhang, B., e,Wang X., 2013. Coupled modeling between
729 geological structurefields and property parameter fields in 3D engineering geological space. Eng. Geol.
730 167, 105–116. https://doi.org/10.1016/j.enggeo.2013.10.016.
731
732
733 **Supplementary data**
734 **Figure captions**
735 **Figure S1** - Location of the additional control points sampled only for analysis of the stable isotopes of
736 water (δ^2H and δ^{18}O), grouped by aquifer. The colour of the symbols is representative of the different
737 aquifers, according to the legend in Fig. 2.

738 **Figure S2** - Stiff diagrams for sampled surface and groundwaters of the Biskra study area, grouped by
739 aquifer. The colour of the Stiff diagram is representative of the different aquifers, according to the legend
740 in Fig. 2.

741 **Figure S3.** Chloride content plotted against δ^2H for water samples collected at the Biskra study area.
742 Diamonds are representative of groundwater samples and are coloured according to the aquifer they were
743 collected from. Blue squares are representative of surface water samples. Data from Chenaker et al. (2017)
744 for two hot springs from the Biskra area are also shown (H Salihine Biskra and H El hadjeb Biskra). The four
745 Groups defined in section 4.2.2 are shown, as well as potential mixing and reactive processes.

746 **Table captions**

747 **Table S1** - Field parameters, major anions, major elements and isotopic data for the samples collected at
748 the Biskra study area (GW = groundwater; SW = surface water; SP = spring; EC = electric conductivity; nd =
749 not determined; na = not available). The different colours represent the different aquifer units.

750 **Table S2** - Results for the additional samples collected at the Biskra study area in May 2013 specifically for
751 analysis of the stable isotopes of water (GW = groundwater; SW = surface water; SP = spring; nd = not
752 determined; na = not available). The different colours represent the different aquifer units.